

Efficient Calculation of the 3-D Rectangular Waveguide Green's Functions Derivatives by the Ewald Method

Antonio Manuel Huéscar de la Cruz, *Student Member, IEEE*, Celia Gómez Molina, Fernando Daniel Quesada Pereira, *Member, IEEE*, Alejandro Álvarez Melcón, *Senior Member, IEEE*, Vicente E. Boria Esbert, *Fellow, IEEE*,

Abstract—In this contribution, the Ewald method has efficiently been applied to accelerate the computation of the rectangular waveguide Green's functions derivatives. Based on previous works, we have outlined new approximation formulae that avoid the evaluation of computationally expensive complementary error functions of complex argument, needed by the Ewald method. This is possible when the internal medium of the rectangular waveguide is homogeneous and lossless. On the other hand, different convergence numerical studies have been carried out, showing a similar convergence rate for computing the original Green's functions and their derivatives. Moreover, we have checked that the computational time is only slightly increased for obtaining the derivatives as compared to the original Green's functions, after the application of these new techniques. The new derived expressions are useful for the evaluation of electromagnetic fields, the characterization of dielectric materials and step discontinuities between rectangular waveguides, and the analysis of rectangular cavities using integral equation formulations. For validation, the electric field produced by a surface electric current density with a rectangular pulse distribution has been evaluated, using the new proposed expressions. These results have been compared to simulations provided by a full-wave finite elements commercial software to verify their correctness, exhibiting a good agreement.

Index Terms—Electric field evaluation, Ewald method, Green's function, integral equation, rectangular waveguide, splitting parameter (E).

Manuscript received February 16, 2023; revised XXX X, 2023; accepted XXXX X, 2023. Date of publication XXXX, X, 2023; date of current version XXXX X, 2023. This work was supported by the Spanish Ministerio de Ciencia e Innovación (Grant MCIN/AEI/10.13039/501100011033) in the framework of the R&D coordinated projects “Green an Efficient Technologies for Advanced Telecommunication Systems (GRETAS)” with Ref. PID2019-103982RB-C42, “Advanced Design of New High Frequency Components in Compact Waveguide Technologies for Future Telecommunication Satellites (GUIDESAT)” with Ref. PID2019-103982RB-C41, from the Agencia Estatal de Investigación, European Union Next Generation Funds in the project “Antennas and circuits for Efficient Wireless Sensor Networks using Low-orbit Satellites (ARIELS)” with Ref. TED2021-129196B-C42, and from Fundación Séneca, Agencia de Ciencia y Tecnología de la Región de Murcia, Spain, under project 22076/PI/22, which is included in the Regional Program for the Promotion of the Research (2022), “Componentes radiantes y de filtrado de microondas para satélites emergentes”. (*Corresponding author: Fernando Daniel Quesada Pereira*).

Antonio Manuel Huéscar de la Cruz, Fernando D. Quesada Pereira and Alejandro Alvarez Melcon are with the Department of Communications and Information Technologies, Universidad Politécnica de Cartagena, 30202 Cartagena, Spain (e-mail: fernando.quesada@upct.es).

Celia Gómez Molina is with Erzia Technologies, 39012 Santander, Cantabria, Spain

Vicente E. Boria Esbert is with the Research Development Institute on Telecommunication and Multimedia Applications, Universitat Politècnica de València, Valencia, Spain.

I. INTRODUCTION

A VAST number of waveguide technology devices used in communication systems [1], has encouraged the development of efficient numerical techniques to obtain their electrical responses along with their internal electromagnetic field distributions. In addition, these devices can be composed of a given number of arbitrarily shaped metallic and/or dielectric elements [2], [3]. Integral equation techniques [4] are one of the most numerically efficient alternatives for the analysis of this kind of structures, since they can significantly reduce the number of unknowns required to obtain accurate results. This advantage is mainly due to the use of Green's functions in the integral equation kernel, that effectively take into account the boundary conditions on the waveguide walls, and limit the numerical solution to cope with the internal discontinuities. On the other hand, the presence of homogeneous material objects, such as dielectric resonators or metal posts, can conveniently be modelled by the Surface Equivalence Principle [5]. Moreover, arbitrarily shaped step discontinuities between rectangular waveguides can be modelled by equivalent magnetic current densities defined on their connecting boundary after enforcing the continuity of the tangent magnetic field [4]. These features, along with the need to compute the electromagnetic fields distribution for design purposes, or to model some important physical phenomena (e.g. multipactor and corona, [7], [8]), associated with power handling capabilities of microwave devices, require the evaluation of Green's functions derivatives in the integral equation framework.

Most Green's functions are expressed mathematically as slowly converging series, either in the spectral domain or in the spatial domain. In these cases, it is necessary to apply series acceleration techniques. A review of different acceleration techniques for Green's functions corresponding to two-dimensional (2-D) and three-dimensional (3-D) problems with 1-D and 2-D spatial periodicities is presented in [9]. These techniques include commonly used procedures such as the Kummer decomposition, the Shanks transformation or the Ewald method [10], the latter being the most advantageous for this type of structures. On the other hand, the Kummer transform is a simple and rather generic technique, which allows to accelerate a slowly converging series by decomposing it into two parts, which can be evaluated analytically or computed efficiently [11], [12]. Nevertheless, in previous works we could see some of the drawbacks of the Kummer's transformation,

mixed with the Shanks' transform [13]. In fact, when the distance to the source is very small the method starts to lose accuracy.

Ewald method is based on splitting the original series into two parts, one in the spatial domain and the other in the spectral domain. Ewald method can be used to accelerate different types of Green's functions, as in [14], where it was applied to the Green's function of a 2-D periodically distributed matrix of 2-D linear sources, and in [15], where Ewald method is shown for the evaluation of the Green's functions of 2-D rectangular cavities in a very efficient way. For the analysis of more complex 3-D problems, other works can be found such as the one shown in [16], where the Ewald method is used to accelerate the Green's functions corresponding to a rectangular cavity. Another more elaborate example can be found in [17], where authors have used hybrid strategies to accelerate the evaluation of the rectangular cavity Green's functions. Depending on whether the distance between the source and the observation points is small or sufficiently large, in [17] they used respectively the Ewald method or a direct summation in the spectral domain. One can also look at the case of [18], where the Ewald method is combined with the Boundary Integral - Resonant Mode Expansion (BI-RME) technique to evaluate the Green's function of the rectangular cavity. In that work, the Ewald method was applied to the Coulomb gauge static Green's function of the rectangular cavity using the BI-RME method. Another option to accelerate the Green's functions, but this time specifically applied to rectangular waveguides, is to try to exploit a combination of the Kummer's transformation and the Ewald method as done in [19]. For this purpose, the Green's functions are split into a frequency-independent static part, evaluated efficiently with the Ewald Method, along with a dynamic counterpart computed accurately with the Kummer's transformation, except for distant source and observation points which require a summation by parts technique to maintain the precision [20]. As far as we know, the evaluation of the rectangular waveguide Green's functions was not discussed in any of these previous works.

In this work, we focus on the extension of the Ewald method [21] to the efficient evaluation of the rectangular waveguide Green's functions derivatives. As a starting point, the formulation presented in [22], which discusses the application of the Ewald method to accelerate the non-derivative rectangular waveguide Green's functions, will be used as reference. An important contribution in [21] was the development of useful approximations that do not depend on the evaluation of inefficient complementary error functions of complex argument for computing the Green's functions. In this sense, we have found new especially suited expressions that permit calculating the Green's functions derivatives with only fast real argument complementary error functions. The formulation uses some function transformations and series expansions reported in [22]. Moreover, we have dynamically chosen the optimum Ewald Method splitting parameter (E_{opt}), that is key for its convergence performance, as in [23], [24].

This work is organized as follows. First, in Section II the spectral and spatial domain forms of the rectangular waveguide

3-D Green's function derivatives are presented. Moreover, the Ewald method is applied to accelerate the calculation of both, where some convenient expressions have been found to avoid the evaluation of numerically expensive complementary error functions of complex argument. Some convergence studies have also been carried out, in order to show the performance of Ewald method for evaluating derivatives for different configurations. In Section III, we will describe how to evaluate the electric field using a mixed-potential formulation combined with the outlined Green's functions [21] and their derivatives. The results are validated with commercial software ANSYS HFSS [25]. Finally, Section IV presents the main conclusions and some further research work in this area.

II. GREEN'S FUNCTIONS DERIVATIVES

In this section, the procedure to efficiently compute the rectangular waveguide Green's functions derivatives by using the Ewald method will be outlined. It should be recalled that these derivatives are of great importance in the evaluation of electromagnetic fields to study high-power phenomena, and also for the analysis of waveguides with metallic and/or dielectric elements of arbitrary shape by means of the surface equivalence principle [5], [26]–[28]. On the other hand, as discussed in the introduction, and as will be seen throughout this section, the direct evaluation of these derivatives after the application of the Ewald method is not computationally efficient due to complementary error functions of complex argument, required in the formulation. One of the motivations of this contribution will be the extension of some of the ideas presented in [21] to the evaluation of the rectangular waveguide Green's functions derivatives. Additionally, in this work, it will also be shown how to choose the optimal values of the Splitting Parameter (E) from the work developed in [23], [24]. Finally, to conclude this section, some convergence analyses will be carried out to validate the developed formulation, and to verify its computational efficiency with respect to the non-derivatives functions presented in [21].

A. Evaluation of Rectangular Waveguide Green's Functions Derivatives by the Ewald Method

Starting from the original expressions presented in [21], and following the methodology used in [29] to evaluate the derivatives of the Green's function of a rectangular waveguide as shown in Fig. 1, it is not difficult to obtain the derivatives of all potentials. This derivatives can be written in two different ways. The first form corresponds to an infinite series of modal functions in the spectral domain, whereas the second is defined as a two-dimensional distribution of discrete images in the spatial domain.

The generic expression in the spectral domain can be written as follows,

$$\frac{\partial G^{spec}}{\partial p} = \frac{\vartheta}{2ab} \sum_{m,n=0}^{\infty} \nu_p \frac{\epsilon_m \epsilon_n}{\gamma_{mn}} e^{-\gamma_{mn}|z-z'|} \cdot g_m(k_x x) r_m(k_x x') q_n(k_y y) s_n(k_y y'), \quad (1)$$

where g_m , r_m , q_n and s_n are trigonometric functions, ϑ is a constant related to the material medium filling the rectangular

TABLE I
SOME TERMS OF THE RECTANGULAR WAVEGUIDE GREEN'S FUNCTIONS DERIVATIVES IN THE SPECTRAL DOMAIN FOR THE MAGNETIC VECTOR POTENTIAL (\overline{G}_A) AND ELECTRIC SCALAR POTENTIAL (G_V).

ϑ		ν_p	$g_m(k_x x)$	$r_m(k_x x')$	$q_n(k_y y)$	$s_n(k_y y')$
$\frac{\partial G_A^{zz}}{\partial x}, \frac{\partial G_V}{\partial x}$	$\mu, \frac{1}{\epsilon}$	k_x	$\cos(k_x x)$	$\sin(k_x x')$	$\sin(k_y y)$	$\sin(k_y y')$
$\frac{\partial G_A^{zz}}{\partial y}, \frac{\partial G_V}{\partial y}$	$\mu, \frac{1}{\epsilon}$	k_y	$\sin(k_x x)$	$\sin(k_x x')$	$\cos(k_y y)$	$\sin(k_y y')$
$\frac{\partial G_A^{zz}}{\partial z}, \frac{\partial G_V}{\partial z}$	$-\mu, \frac{1}{\epsilon}$	$\gamma_{mn} \operatorname{sgn}(z - z')$	$\sin(k_x x)$	$\sin(k_x x')$	$\sin(k_y y)$	$\sin(k_y y')$

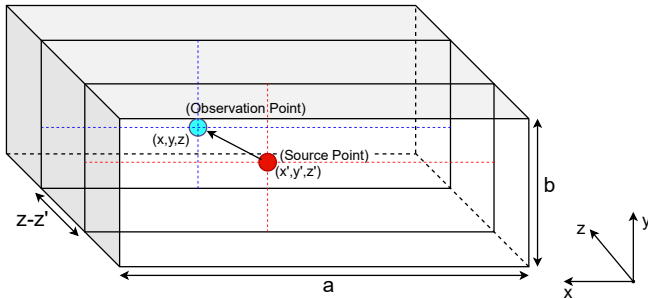


Fig. 1. Sketch of a rectangular waveguide, with dimensions $a \times b$ in the (x,y) plane, for source and observation points that are separated by a distance $|z - z'|$ along the propagation axis.

waveguide (see Table I) and $p = x, y$ or z . Moreover, γ_{mn}^2 , k_x , k_y and ϵ_m are defined as:

$$\begin{aligned} \gamma_{mn}^2 &= k_x^2 + k_y^2 - k^2; \\ k_x^2 &= \left(\frac{m\pi}{a}\right)^2; \quad k_y^2 = \left(\frac{n\pi}{b}\right)^2; \\ \epsilon_m &= \begin{cases} 1, & m = 0 \\ 2, & m \neq 0 \end{cases}. \end{aligned} \quad (2)$$

On the other hand, the spatial domain expressions can be written as:

$$\frac{\partial G^{spat}}{\partial p} = \frac{-\vartheta}{4\pi} \sum_{m,n=-\infty}^{\infty} \sum_{i=0}^3 A_i^{\alpha\alpha} \frac{B_p e^{-jkR_{i,mn}}}{R_{i,mn}^2} \left(\frac{1}{R_{i,mn}} + jk \right), \quad (3)$$

where B_p and $R_{i,mn}$ have the following form:

$$\begin{aligned} B_x &= X_i + 2ma, \quad B_y = Y_i + 2nb, \quad B_z = z - z' \\ R_{i,mn} &= \sqrt{(X_i + 2ma)^2 + (Y_i + 2nb)^2 + (z - z')^2} \\ X_i &= \begin{cases} x - x', & i = 0, 1 \\ x + x', & i = 2, 3 \end{cases} \\ Y_i &= \begin{cases} y - y', & i = 0, 2 \\ y + y', & i = 1, 3 \end{cases} \end{aligned} \quad (4)$$

In the previous equations, $k = \omega\sqrt{\mu\epsilon}$ is the medium wave number, a and b are respectively the width and height of the rectangular waveguide, whereas ν and $A_i^{\alpha,\alpha}$ are shown in Table II. In addition, α can take x, y or z values.

The rectangular waveguide Green's functions and their derivatives can efficiently be evaluated by means of the Ewald method, which is based on the sum of two different contributions, namely the spatial and spectral terms. These terms,

TABLE II
TERMS OF RECTANGULAR WAVEGUIDE GREEN'S FUNCTIONS DERIVATIVES IN THE SPATIAL DOMAIN FOR THE MAGNETIC VECTOR POTENTIAL (\overline{G}_A), ELECTRIC VECTOR POTENTIAL (\overline{G}_F), ELECTRIC SCALAR POTENTIAL (G_V) AND MAGNETIC SCALAR POTENTIAL (G_W), WHERE $p = x, y$ OR z .

ϑ	A_i^{xx}	A_i^{yy}	A_i^{zz}
$\frac{\partial G_A^{\alpha\alpha}}{\partial p}$	$\mu \begin{cases} +1, & i=0,2 \\ -1, & i=1,3 \end{cases}$	$\begin{cases} +1, & i=0,1 \\ -1, & i=2,3 \end{cases}$	$\begin{cases} +1, & i=0,3 \\ -1, & i=1,2 \end{cases}$
$\frac{\partial G_F^{\alpha\alpha}}{\partial p}$	$\epsilon \begin{cases} +1, & i=0,1 \\ -1, & i=2,3 \end{cases}$	$\begin{cases} +1, & i=0,2 \\ -1, & i=1,3 \end{cases}$	$+1 = 0, 1, 2, 3$
ϑ	A_i		
$\frac{\partial G_V}{\partial p}$	$\frac{1}{\epsilon} \begin{cases} +1, & i=0,3 \\ -1, & i=1,2 \end{cases}$		
$\frac{\partial G_W}{\partial p}$	$\frac{1}{\mu}$	$+1 = 0, 1, 2, 3$	

which are conveniently weighted by the so called ‘‘Splitting Parameter’’ (E) [23], are shown below:

$$\frac{\partial G_{\text{Ewald}}}{\partial p} = \frac{\partial G_{\text{Ewald}}^{\text{spec}}}{\partial p} + \frac{\partial G_{\text{Ewald}}^{\text{spat}}}{\partial p} \quad (5)$$

The first term $\left(\frac{\partial G_{\text{Ewald}}^{\text{spec}}}{\partial p}\right)$ is related to the spectral domain modal expansion, whereas the second $\left(\frac{\partial G_{\text{Ewald}}^{\text{spat}}}{\partial p}\right)$ relates to the spatial domain images expansion of the Green's function derivatives in a rectangular waveguide.

The spectral domain derivatives, corresponding to the first term, can be written as follows:

$$\begin{aligned} \frac{\partial G_{\text{Ewald}}^{\text{spec}}}{\partial p} &= \frac{\vartheta}{4ab} \sum_{m,n=0}^{\infty} \nu_p \cdot \frac{\epsilon_m \epsilon_n}{\gamma_{mn}} \cdot g_{\text{ewald}}(z, z', E) \\ &\quad \cdot g_m(k_x x) p_n(k_x x') q_m(k_y y) s_n(k_y y'), \end{aligned} \quad (6)$$

where ν_p and $g_{\text{ewald}}(z, z', E)$ depend on the partial derivative to be evaluated.

For the evaluation of the partial derivatives with respect to $p = x$ and $p = y$, the constants and functions in (6) are particularized as follows,

$$\begin{aligned} \nu_x &= k_x, \\ \nu_y &= k_y, \\ g_{\text{ewald}}(z, z', E) &= g(|z - z'|, \gamma_{mn}, E), \end{aligned} \quad (7)$$

where $g(|z - z'|, \gamma_{mn}, E)$ can be expressed as follows,

$$\begin{aligned} g(|z - z'|, \gamma_{mn}, E) &\equiv e^{\gamma_{mn}(z-z')} \operatorname{erfc}\left(\frac{\gamma_{mn}}{2E} + (z - z')E\right) \\ &+ e^{-\gamma_{mn}(z-z')} \operatorname{erfc}\left(\frac{\gamma_{mn}}{2E} - (z - z')E\right), \end{aligned} \quad (8)$$

and erfc is the complementary error function of complex argument.

On the other hand, for the derivatives with respect to the longitudinal direction $p = z$, and applying the properties of error functions shown in [22], these terms take the next form:

$$\begin{aligned} \nu_z &= 1, \\ g_{\text{ewald}}(z, z', E) &= g'(|z - z'|, \gamma_{mn}, E), \end{aligned} \quad (9)$$

where, in turn, $g'(|z - z'|, \gamma_{mn}, E)$ is expressed as follows:

$$\begin{aligned} g'(|z - z'|, \gamma_{mn}, E) &\equiv \gamma_{mn} e^{\gamma_{mn}(z-z')} \operatorname{erfc}\left(\frac{\gamma_{mn}}{2E} + (z - z')E\right) \\ &- \gamma_{mn} e^{-\gamma_{mn}(z-z')} \operatorname{erfc}\left(\frac{\gamma_{mn}}{2E} - (z - z')E\right) \\ &+ \left(\frac{2E}{\sqrt{\pi}}\right) e^{-\gamma_{mn}(z-z') - (\gamma_{mn}/(2E) - (z-z')E)^2} \\ &- \left(\frac{2E}{\sqrt{\pi}}\right) e^{\gamma_{mn}(z-z') - (\gamma_{mn}/(2E) + (z-z')E)^2}. \end{aligned} \quad (10)$$

Moreover, the spatial domain contribution derivatives can be expressed as shown next:

$$\begin{aligned} \frac{\partial G_{\text{Ewald}}^{\text{spat}}}{\partial p} &= \frac{\vartheta}{8\pi} \sum_{m,n=-\infty}^{\infty} \sum_{i=0}^3 A_i^{\alpha\alpha} \left[\frac{f'_p(R_{i,mn}, E, k)}{R_{i,mn}} \right. \\ &\left. - \frac{f(R_{i,mn}, E, k)}{R_{i,mn}^2} \frac{\partial R_{i,mn}}{\partial p} \right], \end{aligned} \quad (11)$$

being $f(R_{i,mn}, E, k)$, $f'_p(R_{i,mn}, E, k)$ and $\partial R_{i,mn}/\partial p$:

$$\begin{aligned} f(R_{i,mn}, E, k) &\equiv e^{-jkR_{i,mn}} \operatorname{erfc}\left(R_{i,mn}E - \frac{jk}{2E}\right) \\ &+ e^{jkR_{i,mn}} \operatorname{erfc}\left(R_{i,mn}E + \frac{jk}{2E}\right), \end{aligned} \quad (12)$$

$$\begin{aligned} f'_p(R_{i,mn}, E, k) &\equiv -jk \frac{\partial R_{i,mn}}{\partial p} e^{-jkR_{i,mn}} \operatorname{erfc}\left(R_{i,mn}E - \frac{jk}{2E}\right) \\ &+ jk \frac{\partial R_{i,mn}}{\partial p} e^{jkR_{i,mn}} \operatorname{erfc}\left(R_{i,mn}E + \frac{jk}{2E}\right) \\ &- \left(\frac{4E}{\sqrt{\pi}}\right) \frac{\partial R_{i,mn}}{\partial p} e^{\left(\frac{k}{2E}\right)^2 - (R_{i,mn}E)^2}, \end{aligned} \quad (13)$$

$$\begin{aligned} \frac{\partial R_{i,mn}}{\partial x} &= \frac{X_i + 2ma}{R_{i,mn}}, \quad \frac{\partial R_{i,mn}}{\partial y} = \frac{Y_i + 2nb}{R_{i,mn}}, \\ \frac{\partial R_{i,mn}}{\partial z} &= \frac{z - z'}{R_{i,mn}}. \end{aligned} \quad (14)$$

In most practical situations, the medium filling the rectangular waveguide can be modelled as homogeneous and lossless. Consequently, the previously outlined expressions

can be simplified to reduce the computational cost associated to complementary error functions of complex argument. Therefore, as in [21], the complex conjugate property is employed. This property is only applied for the derivatives of the spatial domain expansion, and for the propagative modes in the derivatives of the spectral domain counterpart, since the evaluation of the remaining terms below cutoff in expressions (8) and (10) is computationally efficient. This is because the argument of the complementary error functions is real. Therefore, the only change in the expressions with respect to the derivatives presented above will come in $g'(|z - z'|, \gamma_{mn}, E)$ when the derivative is with respect to z and in $f'_p(R_{i,mn}, E, k)$, thus leading to the next results:

$$\begin{aligned} g'(|z - z'|, \gamma_{mn}, E) &= 2jk_{zmn} \left\{ -e^{jk_{zmn}(z-z')} + \Re \left[e^{jk_{zmn}(z-z')} \operatorname{erfc}\left(\frac{jk_{zmn}}{2E} + (z - z')E\right) \right] \right\} \\ &- \frac{2E}{\sqrt{\pi}} e^{jk_{zmn}(z-z') - \left(\frac{jk_{zmn}}{2E} + (z-z')E\right)^2} \\ &+ \frac{2E}{\sqrt{\pi}} e^{-jk_{zmn}(z-z') - \left(\frac{jk_{zmn}}{2E} - (z-z')E\right)^2}, \end{aligned} \quad (15)$$

$$\begin{aligned} f'_p(R_{i,mn}, E, k) &= -2k \frac{\partial R_{i,mn}}{\partial p} \Re \left[e^{jkR_{i,mn}} \cdot \operatorname{erfc}\left(R_{i,mn}E + \frac{jk}{2E}\right) \right] - \frac{2E}{\sqrt{\pi}} \frac{\partial R_{i,mn}}{\partial p} \\ &\cdot \left[e^{-jkR_{i,mn} - (R_{i,mn}E - \frac{jk}{2E})^2} + e^{jkR_{i,mn} - (R_{i,mn}E + \frac{jk}{2E})^2} \right], \end{aligned} \quad (16)$$

where $\Re[A]$ designates the real part of a complex number A , and $\Im[A]$ represents its imaginary part.

These simplifications reduce the number of error functions with complex arguments to be evaluated by a factor of two. However, as explained in [21], the computational cost of calculating the remaining complex argument error functions is still high. Therefore, we propose new approximations of the complex argument error function by means of infinite series (see [22, (7.1.29)]), which depend only on the complementary real argument error functions. With the help of these infinite series, we obtain for $\Re\{e^{j2xy} \operatorname{erfc}(x + jy)\}$ and $\Im\{e^{j2xy} \operatorname{erfc}(x + jy)\}$ the same expressions as in [21, (10, 11)]. The detailed procedure for obtaining these expressions can be found in Appendix. It is also worth mentioning that tests have been made with the complex argument complementary error function in order to quantify the difference between the expressions developed in this work and the unaccelerated function. The result we have been obtained for an analysis in which we had one source point and 121 observation points is 6 times slower than in the accelerated function. Another conclusion obtained in these tests is that the difference between the two functions grows as the number of times it has to be evaluated increases. The time degradation is not proportional, which is why this form of acceleration of the complementary error functions of complex argument is so advantageous.

B. Calculation of the Optimum Splitting Parameter (E)

The Splitting Parameter (E) used in the Ewald method is chosen dynamically (see [24, (34)]). The expressions that allow to obtain the optimum E value for each case depend on the rectangular waveguide geometry, frequency and other numerical parameters, as can be seen next:

$$E_{opt} = \max\{E_0, E_1, E_2\} = \max\left\{\sqrt{\frac{\pi}{ab}}, \frac{k_{z10}}{2H}, \frac{k}{2(\zeta Q!)^{\frac{1}{2Q}}}\right\}, \quad (17)$$

where k_{z10} is the propagation constant of the first propagating mode, k is the medium wave number, H is the maximum allowed exponent that avoids numerical instabilities, whose value, for our specific cases after a series of tests, is 3 [24], ζ is the desired error, and Q is the number of terms needed to achieve convergence.

C. Green's Functions Derivatives: Convergence and Computational Time

In order to test the numerical performance of the proposed Ewald method acceleration technique, for evaluating the rectangular waveguide Green's functions derivatives, we have used as benchmark a standard WR-90 ($a = 22.86 \text{ mm} \times b = 10.16 \text{ mm}$) rectangular waveguide at $f = 10.2 \text{ GHz}$ in X-band (see Fig. 1). Furthermore, the computational times were obtained on a computer with an Intel Core i5 processor @2.3 GHz and a RAM memory of 8 GB. For all the convergence analyses that will be shown in this subsection, the reference value, in order to calculate the relative error, has been obtained with a very large number of terms included in the relevant series. For each of the examples, the number of terms needed to obtain the reference value will be shown in captions of Fig. 2 to Fig. 5. Figure 2 shows the convergence of the derivative with respect to the propagation direction z of the electrical scalar potential Green's function (G_V), using the direct modal expansion (1). As can be seen in Fig. 2, the convergence is seriously degraded for short electrical distances between source and observation points along the propagation axis $|z - z'|$. This is due to the exponential term in (1) that strongly influences the convergence rate depending on $|z - z'|$. For the x and y variables, the convergence pattern is very similar. For this reason, these derivatives with respect to these variables are not included in the graph.

In the case of the derivatives computed by using the direct spatial image expansion, the result is considerably worse, as the denominator terms (3) degrade the convergent effect of the exponential factor. As a consequence, the results of the summation of this spatial image series never achieve adequate accuracy to be practically usable for the evaluation of these Green's functions. For this reason, the computational cost of using these spatial domain expressions would be unfeasible for the analysis of practical circuits.

Next, we have studied the numerical convergence of the electric scalar potential derivative $\partial G_V / \partial z$, as a function of the number of terms used in (6) for evaluating the spectral domain Ewald method counterpart (see Fig. 3). As can be seen,

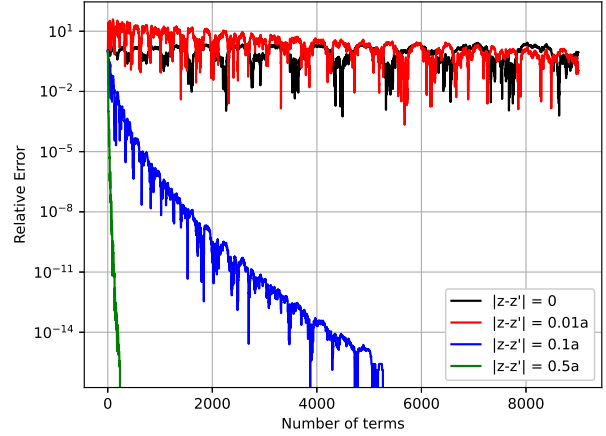


Fig. 2. Convergence of the derivative of the electric scalar potential Green's function in the spectral domain ($\partial G_V / \partial z$) using (1), where the abscises represent the number of summed modal terms, being each curve provided for a different $|z - z'|$ distance ($x' = 13 \text{ mm}$, $y' = 5.5 \text{ mm}$; $x = 9 \text{ mm}$, $y = 5 \text{ mm}$). The dimensions of the rectangular waveguide are ($a = 22.86 \text{ mm} \times b = 10.16 \text{ mm}$) and the test frequency is $f = 10.2 \text{ GHz}$. The number of terms used for the reference value is 30000.

for a given source (x', y') and observation (x, y) locations in the cross-section and for different distances $|z - z'|$ along the propagation axis, only 12 terms lead to a relative error lower than 10^{-6} . On the other hand, we have also checked that only one image layer is needed to achieve convergent results for the spatial domain Ewald method contribution (11). Moreover, the convergence rate exhibits very small dependence with the longitudinal distance from source to observation points $|z - z'|$. With regard to the selection of the optimum splitting parameter E_{opt} , the criteria presented in Section II-B have been followed. Therefore, we can state that using Ewald method, convergence can be achieved for any distance $|z - z'|$ with a low computational cost.

In the next numerical example (see Fig. 4), we have compared the number of terms required by the Ewald method and the original spectral domain Green's functions (GFs) derivatives to achieve convergent results (relative error $< 10^{-6}$), for a configuration of source and observation points located at a relatively far distance along the propagation direction ($|z - z'| = 0.5a$). In this situation, for a relative error of 10^{-6} , 57 terms are needed by the original GF spectral domain representation, whereas the Ewald method meets the same relative error with only 12 terms. On the other hand, only for very large $|z - z'|$ distances, the original spectral domain GF representation is more efficient than its Ewald method equivalence, due to its simpler expression (0.25 ms vs 0.84 ms, respectively; see equations (1) and (2), that avoids the evaluation of computationally expensive complementary error functions as required in (5)-(13).

In the last numerical test (see Fig. 5), we have studied the convergence performance of G_V and its different derivatives $\partial G_V / \partial p$, for a particular location of source and observation points. As can be observed in Fig. 5, the convergence rate of G_V and its derivatives is very similar. Nevertheless, the time

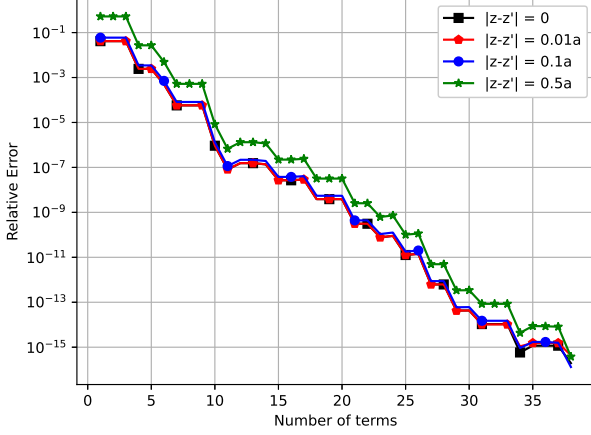


Fig. 3. Convergence of the derivative of the electric scalar potential Green's Function ($\partial G_V/\partial z$) evaluated by the Ewald summation, where the abscises stand for the number of modal terms. Each curve is computed for a different $|z - z'|$ distance. The coordinates of the source and observation point are $x' = 13$ mm, $y' = 5.5$ mm; $x = 9$ mm, $y = 5$ mm, and the dimensions of the rectangular waveguide are ($a = 22.86$ mm \times $b = 10.16$ mm) and the test frequency is $f = 10.2$ GHz. The number of terms used for the reference value is 200.

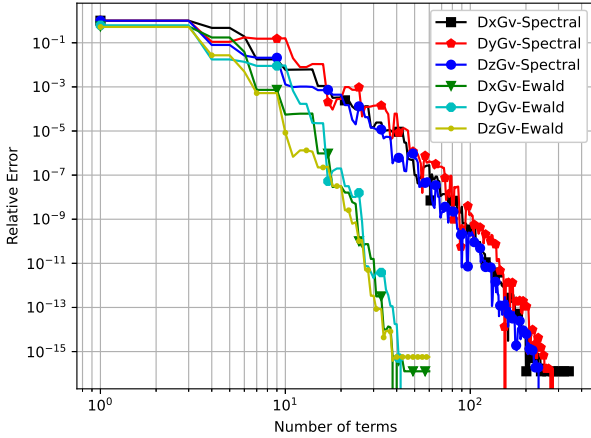


Fig. 4. Convergence of the original modal expansion of the electric scalar potential Green's function derivatives with respect to x , y and z , versus the results provided by the Ewald summation technique ($\partial G_V/\partial x$, $\partial G_V/\partial y$, $\partial G_V/\partial z$). The coordinates of the source and observation point are $x' = 13$ mm, $y' = 5.5$ mm, $x = 9$ mm, $y = 5$ mm; $|z - z'| = 0.5a$, and the dimensions of the rectangular waveguide are ($a = 22.86$ mm \times $b = 10.16$ mm) and the test frequency is $f = 10.2$ GHz. The number of terms used for the reference value is 200 for the Ewald method and 5000 for the spectral summation.

needed for G_V (0.29 ms) is around four times lower than the time required by its derivatives (0.84 ms), due to more complex mathematical expressions involved in the calculations for the last case.

Finally, we have collected in Table III the computational time needed to achieve a relative error less than 10^{-6} during the calculation of 25 observer points equispaced in a cross-section XY plane. The two last columns correspond to two different distances from the source to the observation plane,

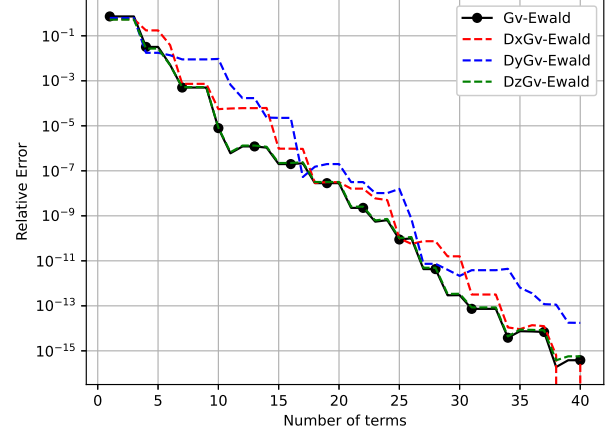


Fig. 5. Convergence of the derivatives of the electric scalar potential Green's Function ($\partial G_V/\partial p$), versus the electric scalar potential Green's Function (G_V), both evaluated by the Ewald method as a function of the number of terms summed in the spectral domain counterpart ($x' = 13$ mm, $y' = 5.5$ mm; $x = 9$ mm, $y = 5$ mm; $|z - z'| = 0.5a$). The dimensions of the rectangular waveguide are ($a = 22.86$ mm \times $b = 10.16$ mm) and the test frequency is $f = 10.2$ GHz. The number of terms used for the reference value is 200.

close ($|z - z'| = 0.01a$) and far ($|z - z'| = 0.5a$) from each other along the propagation axis. As can be seen, the evaluation time needed by the derivatives ∂G_V is higher than that spent computing G_V . However, this difference is small and does not represent a significant overhead for integral equation techniques where these Green's functions are used. Green's functions derivatives are usually needed in the evaluation of the electromagnetic field distributions, in the analysis of dielectric objects by the Surface Equivalence Principle, as well as in the analysis of step discontinuities between rectangular waveguides.

TABLE III

COMPUTATION TIME FOR THE ELECTRIC SCALAR POTENTIAL GREEN'S FUNCTION (G_V) AND ITS DERIVATIVE WITH RESPECT TO THE VARIABLE z ($\partial G_V/\partial z$) WITH A SOURCE POINT AT $x' = 13$ mm, $y' = 5$ mm AND 25 OBSERVATION POINTS EQUISPACED IN A CROSS-SECTION XY PLANE. RESULTS ARE GIVEN FOR A RELATIVE ERROR $< 10^{-6}$. THE DIMENSIONS OF THE RECTANGULAR WAVEGUIDE ARE ($a = 22.86$ mm \times $b = 10.16$ mm) AND $f = 10.2$ GHz.

	$ z - z' = 0.01a$	$ z - z' = 0.5a$
$G_V^{spectral}$	1.103×10^{-2} s	1.420×10^{-4} s
$\partial G_V^{spectral}$	1.346×10^{-2} s	1.859×10^{-4} s
G_V^{Ewald}	2.937×10^{-4} s	2.901×10^{-4} s
∂G_V^{Ewald}	8.168×10^{-4} s	8.251×10^{-4} s

III. ELECTRIC FIELD COMPUTATION

A. Development of the Electric Field Expressions Generated by a Surface Electric Current Density with a Rectangular Pulse Distribution inside a Rectangular Waveguide.

First, we will study how to evaluate the electric field in a given region within the rectangular waveguide. For this, we

will use the expression for the evaluation of the electric field in terms of mixed potentials [26], as follows,

$$\vec{E} = -j\omega\vec{A} - \nabla\phi_e, \quad (18)$$

where ω is the angular frequency, \vec{A} is the magnetic vector potential and ϕ_e is the electric scalar potential.

We then write in more detail (18), where we have to make use of the dyadic magnetic vector potential Green's function of the rectangular waveguide (\vec{G}_A) and the scalar electric potential Green's function (G_V), thus obtaining an expression to calculate the electric field for an arbitrary surface current density distribution. Therefore, taking into account such Green's functions, and also the continuity equation for expressing the charge in terms of a single source of electric current density, we obtain the following expression,

$$\vec{E} = -j\omega \iint \vec{G}_A(\vec{r}, \vec{r}') \vec{J}_s(\vec{r}') dS' + \frac{1}{j\omega} \iint \nabla G_V(\vec{r}, \vec{r}') \nabla' \cdot \vec{J}_s(\vec{r}') dS', \quad (19)$$

where, \vec{r} and \vec{r}' are, respectively, the observation and source position vectors.

In our particular analysis, the excitation will be a constant electric current density within the pulse that can have different orientations, as will be discussed in Section III-B below. It is also possible to use other types of excitations, but in this case we will use the excitation described above for the sake of simplicity in its definition and easiness in comparison to results provided by ANSYS HFSS with an equivalent model. Continuing with the development, it is important to note that when the rectangular current pulse is oriented along the XZ plane (taking into account the model depicted in Fig. 6) the distance along the propagation axis between the source and the observation plane will vary. On the other hand, in the case where the pulse is oriented in the XZ plane, the current density within the pulse may be in the X or Z direction, as it is important to differentiate that the orientation of the current pulse and the direction of the current density within the pulse are two different things.

In this particular example, the excitation will be a rectangular pulse of surface electric current density $\vec{J}_s(\vec{r}')$ of dimensions $l_x \times l_y$, oriented along the y-axis and located at $z'_c = 0$ as shown in Fig. 6,

$$\vec{J}_s(\vec{r}') = \Pi\left(\frac{x' - x'_c}{l_x}\right) \Pi\left(\frac{y' - y'_c}{l_y}\right) \hat{y} \quad (\text{A/m}), \quad (20)$$

where x'_c and y'_c stands for the midpoint of the pulse on each axis, \hat{y} represents the orientation of the current and the Greek alphabet symbol Pi refers to the rectangular current pulse.

The electric field will be evaluated at a set of points located in the XY plane corresponding to the rectangular cross-section of the waveguide, separated from the source by a distance $|z - z'|$ along the propagation axis, as shown in Fig. 6. As can be observed in (19), when the divergence of the current pulse is evaluated, what we obtain are two line integrals. These integrals are defined on the axis perpendicular to the current orientation and on which the pulse is defined. Actually, these

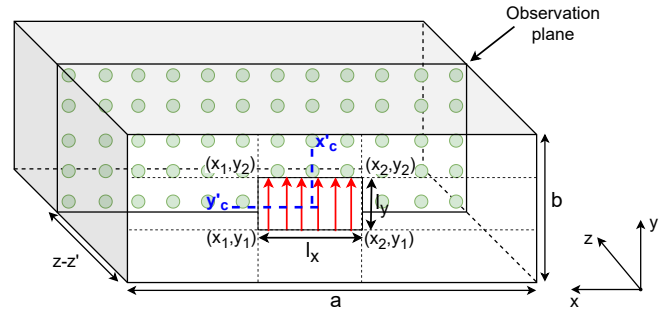


Fig. 6. Sketch of a WR-90 rectangular waveguide ($a = 22.86$ mm \times $b = 10.16$ mm), where a y-oriented surface electric current density with a rectangular pulse distribution in the XY-plane is depicted. The observation plane is separated from the source pulse a distance $|z - z'|$ along the propagation axis.

line integrals correspond to a distribution of spatial deltas defined along the integration line. For the particular case depicted in Fig. 6 (y-oriented electric current pulse defined on XY plane), the resulting line integrals will be evaluated along the x-axis.

To continue, we split the electric field by components and establish the limits of the integrals, which will be determined by the electric current pulse geometry. In this way, the final expression for the electric field components can be written as follows,

$$E_p = -j\omega A_p \int_{x_1}^{x_2} \int_{y_1}^{y_2} G_A^{yy}(\vec{r}, \vec{r}') dy' dx' + \frac{1}{j\omega} \int_{x_1}^{x_2} \frac{\partial G_V(\vec{r}, x', y' = y_1, z' = z'_c)}{\partial p} dx' - \frac{1}{j\omega} \int_{x_1}^{x_2} \frac{\partial G_V(\vec{r}, x', y' = y_2, z' = z'_c)}{\partial p} dx', \quad (21)$$

where $z' = z'_c = 0$ represents the location of the current pulse on the propagation axis, x'_c and y'_c represent the centre point of the current pulse along the x and y axes respectively, and $x_1 = x'_c - \frac{l_x}{2}$, $x_2 = x'_c + \frac{l_x}{2}$, $y_1 = y'_c - \frac{l_y}{2}$, $y_2 = y'_c + \frac{l_y}{2}$. On the other hand the subscript $p = x, y$ or z and A_p will have a value of 1 for $p = y$ and 0 in the other cases.

It should be noted that, if the orientation of the pulse were different, these line integrals would be defined on a different axis. Some of these possible variations of this initial example are explored next in the results Section III-B. Furthermore, with this mixed-potential formulation the magnetic field has also been evaluated, nevertheless for the sake of space the detailed procedure has not been included in this paper.

B. Evaluation of the Electric Field Pattern in a Rectangular Waveguide from a Surface Electric Current Density Pulse Distribution.

In this section, we will evaluate the electric field pattern in a determined observation plane within the rectangular waveguide, produced by a rectangular pulse of surface electric current density as outlined in Section III-A. Furthermore, to verify that the electric field evaluation results obtained in the examples below are correct, they will be compared

to simulated data provided by the full-wave ANSYS HFSS commercial software [25]. On the other hand, the measured computational cost for some of the analyses in this subsection correspond to a computer with an Intel Core i7-6700K processor @4.00 GHz and 40 GB RAM. In this evaluation, we will have to adjust the amplitude of the current used by HFSS, to be equivalent to the pulse current used in our mixed potentials method [30]. To do this we will have to calculate the total current flow along the pulse, so the result obtained is the value by which we have to multiply the current in the ANSYS HFSS excitation model to make it comparable to the method of mixed-potential proposed in this paper. In these examples, it would be more illustrative to check the components of the electric field separately, as there will be components with evanescent behaviour. For example, in the case of Fig. 7, the direction of the current inside the pulse is oriented along the y -axis, so the components E_x and E_z will have an evanescent behavior. In the examples below, the working frequency is $f = 17$ GHz, where we have 4 propagating modes and the distance $|z - z'| = 0.5$ mm. Therefore, following the example of Fig. 7, E_y will have a propagative behaviour, since, as seen in (21), it is the only component with a non-zero contribution from the magnetic vector potential. To make the validation more general, Fig. 8 shows the E_y component radiated by a current pulse, but this time with the surface current density oriented along the x -axis. In this case the contribution of the magnetic vector potential will be zero, so E_y and E_z will have evanescent behavior. Due to the propagation of higher-order modes, this component-by-component evaluation will allow us to prove that each and every one of the components of the electric field evaluated by using the outlined Green's functions and their derivatives are correct. In fact, in the comparisons shown in Fig. 7 and 8, it can be seen that this mixed potentials method correctly compares the results with those provided by ANSYS HFSS. Moreover, all the aforementioned evanescent components are of great importance in this work, since, as shown in Section III-A, close to the source their main contribution comes from the derivatives of the electric scalar potential Green's function. This shows the importance of this work, since the derived theory allows a fast solution for the scalar Green's function derivatives.

On the other hand, to show the accuracy of the method used to evaluate the electric field, we will calculate the relative root mean square error of the total field, for a set of points uniformly distributed in a given XY plane located at a distance “ z ” along the propagation axis, between the results obtained by our method and those provided by the commercial software based on finite elements ANSYS HFSS [25]. Tables IV, V and VI show how the relative root mean squared error of the total electric field (\vec{E}_{total}) varies, if the accuracy of the ANSYS HFSS simulations is increased, if the distance between source and observation plane is modified or if the working frequency is altered, respectively. In Table IV to increase the accuracy, we will make use of the ANSYS HFSS “Lambda Refinement” parameter (λ_{target}) [25]. The size of the tetrahedra will depend on the parameter λ_{target} and the working frequency selected to obtain the solution. To improve accuracy, we decrease the

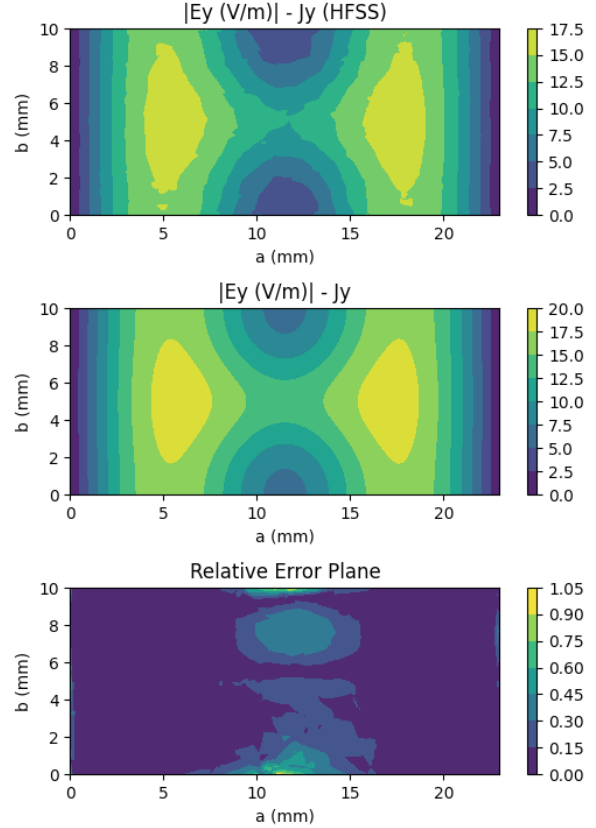


Fig. 7. Comparison between data retrieved from ANSYS HFSS (first) and the mixed-potential evaluation (second), of the E_y component of the E-field for an XY-plane surface electric current density with a rectangular pulse distribution oriented along the y -axis ($\vec{J}_s = J_y \hat{y}$). The third image refers to the relative error distribution between both electric field distributions shown in this same figure. The ANSYS HFSS result taken as a reference has been calculated for a $\lambda_{target} = 0.1$. The operation frequency is $f = 17$ GHz. The rectangular waveguide is a WR-90 ($a = 22.86$ mm \times $b = 10.16$ mm).

λ_{target} value, so that in the final mesh the electrical size of the finite elements mesh tetrahedra is smaller. This procedure will be carried out until the machine's computational resources are pushed to the limit, so that the result obtained for this limit example will be considered as the optimum for calculating the relative error in the subsequent examples.

TABLE IV
RELATIVE ERROR OF THE TOTAL ELECTRIC FIELD (\vec{E}_{total}) FOR DIFFERENT ACCURACY VALUES IN HFSS (λ_{target}). IN THIS EXAMPLE, THE PULSE IS DEFINED IN THE XY PLANE, WITH A SURFACE CURRENT DENSITY DIRECTION ON THE y -AXIS ($\vec{J}_s = J_y \hat{y}$) AND $l_x = 4$ MM \times $l_y = 2$ MM). THE WORKING FREQUENCY IS $f = 17$ GHz AND THE DISTANCE BETWEEN SOURCE AND OBSERVATION ALONG THE PROPAGATION AXIS $|z - z'| = 5$ MM.

λ_{target}	0.3	0.25	0.2	0.15	0.1
Relative Error	0.35	0.22	0.20	0.16	0.14

In Table IV, it can be seen that decreasing the λ_{target} value results in a smaller relative error, due to a higher number of tetrahedra, which allows a more accurate analysis in HFSS.

is automatically recalculated as the frequency is increased.

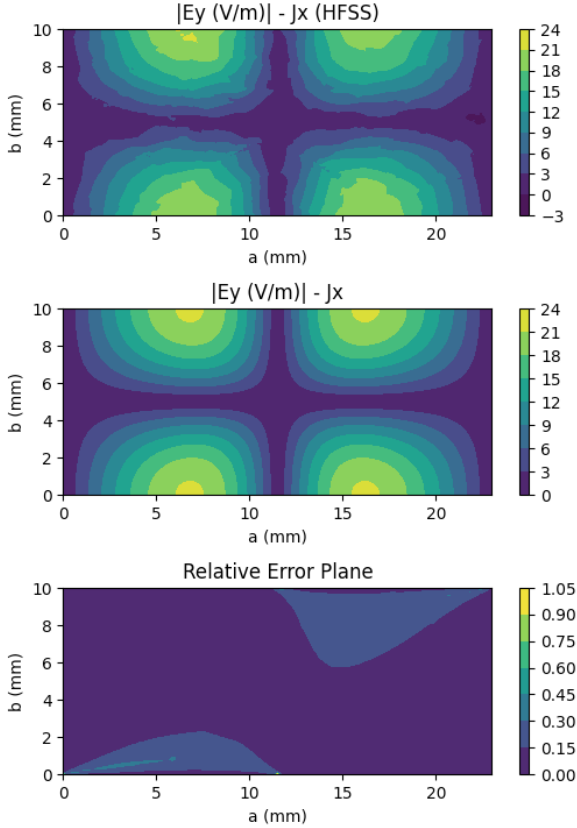


Fig. 8. Comparison between results provided by ANSYS HFSS and the mixed-potential evaluation, of the E_y component of the E-field for an XY-plane surface current density pulse oriented along the x -axis ($\vec{J}_s = J_x \hat{x}$). The third image refers to the relative error distribution between the two electric field distributions shown in this same figure. The ANSYS HFSS result taken as a reference has been calculated for a $\lambda_{target} = 0.1$. The working frequency is $f = 17$ GHz. The rectangular waveguide is a WR-90 ($a = 22.86$ mm \times $b = 10.16$ mm). We remark that in this calculation only derivatives of the electric scalar potential Green functions are involved.

However, it is important to note that increasing the accuracy of these analyses in this type of commercial software is very computationally expensive. On the other hand, in Table V, taking a fixed value of frequency and a $\lambda_{target} = 0.1$ (which is the value we take as the precision reference), we can see how the relative error varies when the observation plane moves away along the propagation axis. In this Table, the relative error grows for closer distances because of the worse accuracy for a given mesh of ANSYS HFSS nearby the source. In fact, the fields have a singular behaviour near the source, which is an additional reason for the worse accuracy achieved. Continuing with the analyses, in Table VI, the variation has been made with respect to frequency. In this case, it can be seen that by choosing a $\lambda_{target} = 0.1$ and being at a relatively far distance from the source, the relative errors remain reasonably low over a wide range of frequencies. For these examples, the number of summed terms in the Ewald method has been increased to maintain good accuracy in the mixed-potential calculations. Likewise, by maintaining a $\lambda_{target} = 0.1$ in ANSYS HFSS, the number of mesh tetrahedra

TABLE V

RELATIVE ERROR OF THE TOTAL ELECTRIC FIELD (\vec{E}_{total}) FOR DIFFERENT DISTANCES BETWEEN SOURCE AND OBSERVATION ALONG THE PROPAGATION AXIS OF $|z - z'|$. IN THIS EXAMPLE THE PULSE IS IN THE XY PLANE, WITH A SURFACE CURRENT DENSITY DIRECTION ON THE y -AXIS ($\vec{J}_s = J_y \hat{y}$ AND $l_x = 4$ MM \times $l_y = 2$ MM). THE CALCULATION IN HFSS FOR $\lambda_{target} = 0.1$ IS TAKEN AS THE REFERENCE SOLUTION TO CALCULATE THE RELATIVE ERRORS. THE WORKING FREQUENCY IS $f = 12$ GHz

$ z - z' $ (mm)	1	3	5	10	20
Relative Error	0.45	0.26	0.11	0.064	0.026

TABLE VI

RELATIVE ERROR OF THE TOTAL ELECTRIC FIELD (\vec{E}_{total}) FOR DIFFERENT FREQUENCIES (f). IN THIS EXAMPLE THE PULSE IS IN THE XY PLANE, WITH A SURFACE CURRENT DENSITY DIRECTION ON THE y -AXIS ($\vec{J}_s = J_y \hat{y}$ AND $l_x = 4$ MM \times $l_y = 2$ MM). THE DISTANCE BETWEEN SOURCE AND OBSERVATION ALONG THE PROPAGATION AXIS $|z - z'| = 5$ MM. THE CALCULATION IN HFSS FOR $\lambda_{target} = 0.1$ IS TAKEN AS THE REFERENCE SOLUTION TO CALCULATE THE RELATIVE ERRORS.

f (GHz)	7	12	20	30	50
Relative Error	0.075	0.11	0.079	0.12	0.10

As it can be seen, to obtain good results in ANSYS HFSS the observation has to be at a somewhat large distance from the source, due to the singularity of the fields near the source.

In the last example included in Table VII, we show the computational times for the analyses in Table VI with the mixed-potential (MP) formulation and with the ANSYS HFSS software.

TABLE VII

COMPUTATIONAL TIME CORRESPONDING TO THE MIXED-POTENTIAL (t_{MP}) FORMULATION AND ANSYS HFSS (t_{HFSS}) FOR DIFFERENT FREQUENCIES (f). IN THIS EXAMPLE THE SURFACE CURRENT DENSITY PULSE IS DEFINED IN THE XY PLANE AND ORIENTED ALONG THE y -AXIS ($\vec{J}_s = J_y \hat{y}$ AND $l_x \times l_y = 4$ MM \times 2 MM). THE DISTANCE BETWEEN SOURCE AND OBSERVATION ALONG THE PROPAGATION AXIS IS $|z - z'| = 5$ MM. THE NUMBER OF POINTS USED IN THIS TEST IS 23331 AND THE CALCULATION IN HFSS FOR $\lambda_{target} = 0.1$ IS TAKEN AS THE REFERENCE SOLUTION TO CALCULATE THE RELATIVE ERRORS.

f (GHz)	7	12	20	30	50
t_{MP}	15.73 s	15.92 s	16.44 s	16.32 s	17.90 s
t_{HFSS}	32.16 s	52.54 s	1 m 25 s	6 m 12 s	29 m 46 s

It can be seen in Table VII that the computation time increases slightly as the analysis increases in frequency, due to the appearance of more propagative modes. This requires the use of the approximations outlined in the Green's functions a greater number of times during the analysis. At this point, it should be remembered that these approximations served to accelerate those complementary error functions of complex argument that appeared for the propagative modes. However, it should be noted that the number of propagating modes appearing in these analyses is not very large, so this is another reason why the computational time does not increase

significantly. On the contrary, when these comparisons are performed with ANSYS HFSS, the computational time increases exponentially, due to the increase in the number of tetrahedra that are recalculated for each frequency. The latter makes the use of ANSYS HFSS very computationally intensive as compared to the technique proposed in this paper.

IV. CONCLUSION

In this work, the 3D dynamic Lorentz gauge potential Green's functions derivatives inside a rectangular waveguide have been efficiently evaluated by using the Ewald method. To do so, infinite series approximations have been used to reduce the computational cost associated to complementary error functions of complex arguments. This approximation technique leads to a quite competitive computational cost for the accurate evaluation of the rectangular waveguide Green's functions derivatives. On the other hand, we have also found a similar convergence pattern for evaluating the direct Green's functions and their derivatives, once the Ewald method is applied. Therefore, the results presented in this contribution could be useful in subsequent research on integral equation formulations, focused on the evaluation of electromagnetic fields, the characterization of dielectric materials inside rectangular waveguides, and the analysis of step discontinuities between rectangular waveguides and cavities. To validate the new formulation, a calculation of the electric field produced by surface current density pulses, using these Green's functions, has also been carried out. A reasonable agreement with results provided by commercial software tools, such as HFSS, has been shown.

APPENDIX

COMPLEMENTARY COMPLEX ARGUMENT ERROR FUNCTIONS

This appendix shows how to evaluate complementary complex argument error functions, using infinite series, which will only depend on complementary real argument error functions [21, (10, 11)]. Using these expansions, $\Re \{e^{j2xy} \operatorname{erfc}(x + jy)\}$ and $\Im \{e^{j2xy} \operatorname{erfc}(x + jy)\}$ can be written as,

$$\begin{aligned} \Re \{e^{j2xy} \operatorname{erfc}(x + jy)\} &= \operatorname{erfc}(x) \cos(2xy) \\ &+ \frac{4x}{\pi} e^{-x^2} \cdot \sum_{n=1}^{\infty} \frac{e^{-\frac{n^2}{4}}}{n^2 + 4x^2} (\cosh(ny) - \cos(2xy)) \\ &+ \frac{e^{-x^2}}{2\pi x} (1 - \cos(2xy)) + \epsilon(x, y), \\ &x = (z - z')E, \quad y = k_z/2E \end{aligned} \quad (22)$$

$$\begin{aligned} \Im \{e^{j2xy} \operatorname{erfc}(x + jy)\} &= \operatorname{erfc}(x) \sin(2xy) \\ &- \frac{2}{\pi} e^{-x^2} \cdot \sum_{n=1}^{\infty} \frac{e^{-\frac{n^2}{4}}}{n^2 + 4x^2} (n \sinh(ny) + 2x \sin(2xy)) \\ &- \frac{e^{-x^2}}{2\pi x} \sin(2xy) + \epsilon(x, y), \\ &x = R_{i,mn}E, \quad y = k/2E \end{aligned} \quad (23)$$

where $\epsilon(x, y)$ is a bounded error term. On the other hand, recall that the values of x and y in (24) and (25) are the arguments of the complementary error function of complex argument shown in (15) and (16).

In (24) and (25), it will be necessary to verify the optimum number of terms used in the summations to achieve the necessary accuracy, but at a much lower computational cost as compared to using the complex-argument complementary error functions. In general, we have verified that good accuracy is obtained with just ten terms in these expansions.

REFERENCES

- [1] R. J. Cameron, C. M. Kudsia, & R. R. Mansour, "Microwave Filters for Communication Systems: Fundamentals, Design and Applications". 2nd ed. Hoboken, NJ, USA: Wiley, Mar. 2018.
- [2] M. Taroncher, A. Vidal, V.E. Boria, S. Marini, S. Cogollos, J. Gil, B. Gimeno "CAD of complex passive devices composed of arbitrarily shaped waveguides using Nyström and BI-RME methods", in *IEEE Trans. Microw. Theory Techn.*, vol. 53, pp. 2153-2163, June 2005, doi: 10.1109/TMTT.2005.848795.
- [3] R. R. Mansour, "Filter technologies for wireless base stations," in *IEEE Microw. Mag.*, vol. 5, no. 1, pp. 68-74, March 2004, doi: 10.1109/MMW.2004.1284945.
- [4] A. F. Peterson, S. L. Ray, R. Mittra, & Institute of Electrical and Electronics Engineers. (1998). "Computational Methods for Electromagnetics" (Vol. 351). New York: IEEE press.
- [5] V. Catina, F. Arndt and J. Brandt, "Hybrid surface integral-equation/mode-matching method for the analysis of dielectric loaded waveguide filters of arbitrary shape," in *IEEE Trans. Microw. Theory Techn.*, vol. 53, no. 11, pp. 3562-3567, Nov. 2005, doi: 10.1109/TMTT.2005.857343.
- [6] F. D. Quesada Pereira, C. Gomez Molina, A. Alvarez Melcon, V. Boria Esbert and M. Guglielmi, "Novel spatial domain integral equation formulation for the Analysis of rectangular waveguide steps close to arbitrarily shaped dielectric and/or conducting posts," *Radio Sci.*, vol. 53, no. 4, pp. 406-419, April 2018, doi: 10.1002/2017RS006429.
- [7] A. Romera Perez, A. Pons Abenza, F. D. Quesada Pereira, J. Hinojosa Jimenez, A. Alvarez Melcon, J. S. Gomez Diaz, "A novel low-pass filter based on dielectric impedance inverters to enhance the multipactor breakdown threshold", *Int. J. Electron. Commun. (AEU)*, vol 143. 2022.
- [8] T. Pinheiro-Ortega, J. Monge, S. Marini, J. Sanz, E. Sorolla, M. Mattes, C. Vicente, J. Gil, V. E. Boria, B. Gimeno, "Microwave corona breakdown prediction in arbitrarily-shaped waveguide based filters", in *IEEE Microw. Wireless Compon. Lett.*, vol. 20, pp. 214-216, April 2010, doi: 10.1109/LMWC.2010.2042555.
- [9] G. Valerio, P. Baccarelli, P. Burghignoli and A. Galli, "Comparative analysis of acceleration techniques for 2-D and 3-D Green's functions in periodic structures along one and two directions," in *IEEE Trans. Antennas Propag.*, vol. 55, no. 6, pp. 1630-1643, June 2007, doi: 10.1109/TAP.2007.897340.
- [10] P. P. Ewald, "Die berechnung optischer und elektrostatischen gitterpotentiale," *Ann. Phys.*, vol. 64, pp. 253-268, 1921.
- [11] F. D. Quesada Pereira et al., "Efficient analysis of arbitrarily shaped inductive obstacles in rectangular waveguides using a surface integral-equation formulation," in *IEEE Trans. Microw. Theory Techn.*, vol. 55, no. 4, pp. 715-721, April 2007, doi: 10.1109/TMTT.2007.893673.
- [12] Y. Leviatan, P. G. Li, A. T. Adams and J. Perini, "Single-post inductive obstacle in rectangular waveguide," in *IEEE Trans. Microw. Theory Techn.*, vol. 31, no. 10, pp. 806-812, Oct. 1983, doi: 10.1109/TMTT.1983.1131610.
- [13] S. Singh and R. Singh, "On the use of Shank's transform to accelerate the summation of slowly converging series," in *IEEE Trans. Microw. Theory Techn.*, vol. 39, no. 3, pp. 608-610, March 1991, doi: 10.1109/22.75314.
- [14] M. -J. Park and B. Lee, "Efficient calculation of the Green's function for 2-D periodic line sources using Ewald method," in *IEEE Antennas Wireless Propag. Lett.*, vol. 8, pp. 565-567, 2009, doi: 10.1109/LAWP.2009.2022652.
- [15] F. D. Quesada Pereira, A. M. Huescar de la Cruz, C. Gómez Molina, A. A. Melcón, and V. E. Boria Esbert, "Integral equation analysis of multi-port H-plane microwave circuits by using 2D rectangular cavity Green's functions accelerated by the Ewald method," *IET Microw., Antennas Propag.*, vol. 17, no. 1, pp. 13-25, 2023.

- [16] Myun-Joo Park, Jongkuk Park and Sangwook Nam, "Efficient calculation of the Green's function for the rectangular cavity," in *IEEE Microw. Guided Wave Lett.*, vol. 8, no. 3, pp. 124-126, March 1998, doi: 10.1109/75.661136.
- [17] M. E. Gruber and T. F. Eibert, "A hybrid Ewald-spectral representation of the rectangular cavity Green's function," *2014 Int. Symp. Electromagn. Compatibility*, 2014, pp. 906-909, doi: 10.1109/EMCEurope.2014.6931032
- [18] M. Bressan, S. Battistutta, M. Bozzi and L. Perregri, "Modeling of inhomogeneous and lossy waveguide components by the segmentation technique combined with the calculation of Green's function by Ewald's method," in *IEEE Trans. Microw. Theory Techn.*, vol. 66, no. 2, pp. 633-642, Feb. 2018, doi: 10.1109/TMTT.2017.2787587.
- [19] F. J. Perez Soler, F. D. Quesada Pereira, D. Cañete Rebenaque, A. Alvarez Melcon and J. R. Mosig, "A novel efficient technique for the calculation of the Green's functions in rectangular waveguides based on accelerated series decomposition," in *IEEE Trans. Antennas Propag.*, vol. 56, no. 10, pp. 3260-3270, Oct. 2008, doi: 10.1109/TAP.2008.929438.
- [20] J. R. Mosig and A. Alvarez Melcon, "The summation-by-parts algorithm—a new efficient technique for the rapid calculation of certain series arising in shielded planar structures," in *IEEE Trans. Microw. Theory Techn.*, vol. 50, no. 1, pp. 215-218, Jan. 2002, doi: 10.1109/22.981269.
- [21] M.J. Park, S. Nam, "Rapid Summation of the Green's Function for the rectangular waveguide," *IEEE Trans. Microw. Theory Techn.*, vol. 46, no. 12, December 1998.
- [22] M. Abramowitz and I. Stegun, Eds., "Handbook of Mathematical Functions," *Solid State Radio Engineering*, New York: Dover, 1970.
- [23] A. Kustepeli and A. Q. Martin, "On the splitting parameter in the Ewald method," in *IEEE Microw. Guided Wave Lett.*, vol. 10, no. 5, pp. 168-170, May 2000, doi: 10.1109/75.850366.
- [24] F. Capolino, D. R. Wilton and W. A. Johnson, "Efficient computation of the 2-D Green's function for 1-D periodic structures using the Ewald method," in *IEEE Trans. Antennas Propag.*, vol. 53, no. 9, pp. 2977-2984, Sept. 2005, doi: 10.1109/TAP.2005.854556.
- [25] ANSYS, *Ansys Electronics Desktop, Release R1*. Canonsburg, Pennsylvania (USA): ANSYS Inc., 2020. [Online]. Available: <https://ansys.com>
- [26] K. Ishibashi and E. Sawado, "A method for the rapidly convergent representation of electromagnetic fields in a rectangular waveguide," in *IEEE Trans. Microw. Theory and Techn.*, vol. 39, no. 10, pp. 1796-1799, Oct. 1991, doi: 10.1109/22.88557.
- [27] V. Catina, F. Arndt and J. Brandt, "A surface integral equation formulation for dielectric post structures in waveguides," in *IEEE MTT-S Int. Microw. Symp. Dig., 2005.*, Long Beach, CA, USA, 2005, pp. 63-66, doi: 10.1109/MWSYM.2005.1616521.
- [28] K. Umashankar, A. Taflove and S. Rao, "Electromagnetic scattering by arbitrary shaped three-dimensional homogeneous lossy dielectric objects," in *IEEE Trans. Antennas Propag.*, vol. 34, no. 6, pp. 758-766, June 1986, doi: 10.1109/TAP.1986.1143894.
- [29] M. Deshpande, "Analysis of discontinuities in a rectangular waveguide using dyadic green's function approach in conjunction with method of moments," 1997.
- [30] J. R. Mosig, "Arbitrarily shaped microstrip structures and their analysis with a mixed potential integral equation," in *IEEE Trans. Microw. Theory Techn.*, vol. 36, no. 2, pp. 314-323, Feb. 1988, doi: 10.1109/22.3520.

BIOGRAPHY SECTION



of analytical and numerical tools for the analysis of microwave circuits in waveguide technology.

Antopnio Manuel Huéscar de la Cruz (IEEE Member) was born in Murcia, Spain, in 1997. He received the bachelor's degree in telecommunication systems and the master's degree in telecommunication engineering from the Technical University of Cartagena (UPCT), Murcia, in 2019 and 2021, respectively.

In 2021 he joined the Department of Information and Communication Technologies of the UPCT as a Researcher, where he currently develops his PhD research activity. He is involved in the development



with the University of California at Davis, Davis, CA, USA, in 2018, and the Politecnico di Milano, Milan, Italy, in 2019. She is involved in the development of analytical and numerical tools for network representations of waveguide and planar discontinuities. Her current scientific interests include the design of microwave filters using different technologies.

Celia Gomez Molina was born in Murcia, Spain, in 1992. She received the bachelor's degree in telecommunication systems from the Technical University of Cartagena (UPCT), Murcia, Spain, in 2014, master's degree in telecommunication engineering from UPCT, in 2016, respectively and Ph.D. degree from UPC) in 2020.

In 2016, she joined the Department of Information Technologies and Communications, UPCT, as a Researcher, where she developed her teaching and Ph.D. research activities. She was a Visiting Student



tag antennas. In 2001, he joined the Department of Communications and Information Technologies, UPCT, as a Research Assistant, and then as an Assistant Professor. In 2005, he was a Visiting Scientist with the University of Pavia, Pavia, Italy. In 2009, he was an Invited Researcher with UPV. In 2011, he became an Associate Professor with UPCT. His current research interest includes integral equation numerical methods for the analysis of antennas and microwave devices, along with microwave filters design and applications.

Fernando Quesada Pereira (Member, IEEE) was born in Murcia, Spain, in 1974. He received the master's degree in telecommunications engineering from the Technical University of Valencia (UPV), Valencia, Spain, in 2000, and the Ph.D. degree from the Technical University of Cartagena (UPCT), Murcia, in 2007.

In 1999, he joined the Department of Radiocommunications, UPV, as a Research Assistant, where he was involved in the development of numerical methods for the analysis of anechoic chambers and



Alejandro Álvarez Melcón (Senior Member, IEEE) was born in Madrid, Spain, in 1965. He received the master's degree in telecommunications engineering from the Technical University of Madrid (UPM), Madrid, in 1991, and the Ph.D. degree in electrical engineering from the ETH Zürich, Lausanne, Switzerland, in 1998.

In 1988, he joined the Department of Signal, Systems and Radiocommunications, UPM, as a Researcher, where he was involved in the design, testing, and measurement of broadband spiral antennas for electromagnetic measurements support equipment. From 1991 to 1993, he was with the Radio Frequency Systems Division, European Space Agency (ESA/ESTEC), Noordwijk, The Netherlands, where he was involved in the development of analytical and numerical tools for the study of waveguide discontinuities, planar transmission lines, and microwave filters. From 1993 to 1995, he was with the Space Division, Industry Alcatel Espacio, Madrid, and also with the ESA, where he collaborated in several ESA/European Space Research and Technology Centre contracts. From 1995 to 1999, he was with the ETH Zürich, École Polytechnique Fédérale de Lausanne, Lausanne, where he was involved with the field of microstrip antennas and printed circuits for space applications. In 2000, he joined the Technical University of Cartagena, Murcia, Spain, where he is currently developing his teaching and research activities. He was an Invited Professor with the Polytechnique Montréal, Montreal, QC, Canada, in 2010, and a Visiting Professor with the University of California at Davis, Davis, CA, USA, from 2017 to 2018.

Dr. Alvarez Melcón was a recipient of the Journée Internationales de Nice Sur les Antennes (JINA) Best Paper Award for the best contribution to the JINA'98 International Symposium on Antennas and the Colegio Oficial de Ingenieros de Telecomunicación Award to the best Ph.D. dissertation in basic information and communication technologies.



Vicente E. Boria (Fellow, IEEE) was born in Valencia, Spain, in 1970. He received the master's degree (Hons.) in telecommunications engineering and the Ph.D. degree in telecommunications engineering from the Universidad Politécnica de Valencia, Valencia, in 1993 and 1997, respectively.

In 1993, he joined the Departamento de Comunicaciones, Universidad Politécnica de Valencia, where he has been a Full Professor since 2003. In 1995 and 1996, he was holding a Spanish trainee position with the European Space Research and Technology Centre, European Space Agency, Noordwijk, The Netherlands, where he was involved in the area of electromagnetic analysis and design of passive waveguide devices. He has authored or coauthored 15 chapters in technical textbooks, 180 articles in refereed international technical journals, and over 200 articles in international conference proceedings. His current research interests are focused on the analysis and automated design of passive components, particularly in filters and multiplexers, several technologies, and the simulation and measurement of power effects in high-frequency devices and systems.

Dr. Boria has been a member of the IEEE Microwave Theory and Techniques Society (IEEE MTT) and the IEEE Antennas and Propagation Society since 1992. He is currently a member of the European Microwave Association (EuMA). He is also an Editorial Board Member of the International Journal of RF and Microwave Computer-Aided Engineering and a member of the Technical Committees of the IEEE-MTT International Microwave Symposium and the European Microwave Conference. He has been the Chair of the 48th European Microwave Conference held in Madrid, Spain. He acts as a regular reviewer of the most relevant IEEE and IET technical journals on his areas of interest. He was an Associate Editor of the IEEE MICROWAVE AND WIRELESS COMPONENTS LETTERS from 2013 to 2018 and the IET Electronics Letters from 2015 to 2018. He currently serves as a Subject Editor of the IET Electronics Letters (Microwaves).